Biochemical Pharmacology, Vol. 57, pp. 1227–1232, 1999.

ISSN 0006-2952/99/$–see front matter
PII S0006-2952(99)00054-4

RAPID COMMUNICATION

Unchanged Cytochrome P450 3A (CYP3A) Expression and Metabolism of Midazolam, Triazolam, and Dexamethasone in *mdr(−/−)* Mouse Liver Microsomes

*Michael D. Perloff, Lisa L. von Moltke, Monette M. Cotreau and David J. Greenblatt**

Department of Pharmacology and Experimental Therapeutics, Tufts University School of Medicine, and Division of Clinical Pharmacology, New England Medical Center Hospital, Boston, MA 02111, U.S.A.

ABSTRACT. P-Glycoprotein (P-gp) and cytochrome P450 3A (CYP3A) share common substrates and expression properties, but the relationship of *mdr1* deficiency to CYP3A-mediated metabolism and protein expression is not established. The *in vitro* kinetic parameters of CYP3A-mediated metabolism of midazolam (MDZ), triazolam (TRZ), and dexamethasone (DEX) were studied in liver microsomes from three *mdr1a(−/−)* mice, one *mdr1a/b(−/−)* mouse, and *mdr1a/b(+/+)* controls. The kinetic profiles of CYP3A-mediated MDZ 4-hydroxylation were not significantly different between *mdr1*-deficient animals and controls. Overall mean (± SEM, N = 8) values were: V_{max}, 0.74 ± 0.05 nmol/min/mg protein; K_m, 28.2 ± 2.7 μM; and estimated intrinsic clearance, 0.026 ± 0.003 mL/min/mg protein. Likewise, rates of formation of α-OH- and 4-OH-TRZ (from 500 μM TRZ), and of DEX metabolites sensitive to ketoconazole inhibition, M1 and M5 (from 20 μM DEX), did not differ between mdr1-deficient and control animals. Immunoquantified microsomal CYP3A protein levels in *mdr1a(−/−)*, *mdr1a/b(−/−)*, and *mdr1a/b(+/+)* mice were not different, with overall mean immunoreactive protein levels of 2.68 ± 0.09 pmol/μg protein. Although CYP3A and P-gp share aspects of activity and expression, disruption of the *mdr1* genes does not affect CYP3A-mediated metabolism or protein expression in the mouse. BIOCHEM PHARMACOL **57**;11:1227–1232, 1999. © 1999 Elsevier Science Inc.

KEY WORDS. *mdr1* gene; P-glycoprotein; cytochrome P450 3A; midazolam; triazolam; dexamethasone

The ATP-dependent xenobiotic transporter P-gp† mediates the export of cytotoxic drugs from cancer cells. The *mdr1* genes, and the corresponding P-gp transporter (as opposed to the *mdr2* gene for a phospholipid flippase), are present and up-regulated in multidrug-resistant cancer cells [1, 2]. P-gp recognizes a wide variety of substrates ranging from chemotherapeutics to antiarrhythmics, with the only shared chemical property being the hydrophobic amphipathic nature of these molecules [3]. Most P-gp substrates have some metabolic relationship with CYP3A, and many drugs are substrates for both [4, 5]. CYP3A isoforms are the major phase I metabolizing enzymes found in human liver, kidney, and small intestine [6]. P-gp substrates that are not direct CYP3A substrates are often products of CYP3A-mediated metabolism [5, 6].

P-gp expression is not limited to cancer cells. It is present in capillary endothelial cells of the brain, testis, adrenal gland, and placental trophoblasts where it serves a barrier function, reducing toxin accumulation [4, 7]. P-gp also plays a role in drug clearance and metabolism, being expressed on the luminal surface of epithelial cells in the kidney proximal tubules, the small and large intestine, and the epithelial surface of biliary hepatocytes [4]. P-gp and CYP3A are co-localized in the enterocyte villus of the small intestine, and the concurrent action of intestinal CYP3A and P-gp creates an absorption barrier that may influence systemic bioavailability of orally administered medications [6, 8].

Along with substrate specificity, co-localization, and drug clearance synergy, *MDR1* and *CYP3A* genes are also located on the same chromosome, with proximal gene loci in humans [9]. Aberrations of the chromosome could affect genetic promoters or repressors and, in turn, expression of P-gp or CYP3A. Both P-gp and CYP3A are expressed and up-regulated in cancer cells [5], and certain known CYP3A inducers also induce P-gp. Although the absolute degree of induction varies, parallel induction by reserpine and rifam-

* Corresponding author: Dr. David J. Greenblatt, Department of Pharmacology and Experimental Therapeutics, Tufts University School of Medicine, Boston, MA 02111. Tel. (617) 636-6997; FAX (617) 636-6738; E-mail: Dgreenblatt@infonet.tufts.edu

† *Abbreviations:* P-gp, P-glycoprotein; CYP, cytochrome P450; MDZ, midazolam; α-OH-MDZ, α-OH-midazolam; 4-OH-MDZ, 4-OH-midazolam; TRZ, triazolam; α-OH-TRZ, α-OH-triazolam; 4-OH-TRZ, 4-OH-triazolam; DEX, dexamethasone; PHR, peak-height ratio; V_{max}, maximum reaction velocity; and K_m, substrate concentration corresponding to 50% V_{max}.

Accepted 19 February 1999.

picin has been demonstrated in human cancer cell lines [10]. Studies evaluating the effects of known CYP3A inducers on P-gp *in vivo* have yielded conflicting results [11–13]. *In vitro* and clinical studies show a significant overlap in drugs that cause inhibition of CYP3A and P-gp [6, 14], relating to the similarity in substrate specificity.

Two *mdr1* genes responsible for drug transport have been cloned in mice, *mdr1a* and *mdr1b*. *mdr1a* is predominately expressed in the intestine, liver, blood capillaries of the brain, and testis, whereas *mdr1b* is found in the adrenal glands, placenta, and (pregnant) uterus [7]. Both *mdr1a* and *mdr1b* are found at similar levels in the kidney [7]. *mdr1a(−/−)* mice have delayed elimination of drugs, such as vinblastine, and accumulate higher systemic concentrations of ivermectin, cyclosporin A, vinblastine, and DEX compared to *mdr1a/b(+/+)* controls [15]. These changes could be due to altered drug disposition caused by the *mdr1a* deficiency, or to a linked alteration in CYP3A expression or activity. This study evaluated the *in vitro* kinetics of CYP3A-mediated drug metabolism and protein expression in liver microsomal preparations from animals having deficient *mdr1* gene expression (P-gp). To evaluate CYP3A-mediated metabolism, the benzodiazepine non-P-gp substrates MDZ and TRZ [5, 10, 16] and the validated P-gp substrate DEX [5, 15] were tested. Because the liver is the organ of interest, *mdr1a*(−/−) mice were tested alongside same species and strain *mdr1a/b*(+/+) controls. As an added control and verification, one *mdr1a/b*(−/−) mouse was tested with a paired *mdr1a/b*(+/+) control animal.

MATERIALS AND METHODS

Chemicals and Antibodies

MDZ, α-OH-MDZ, 4-OH-MDZ, TRZ, α-OH-TRZ, 4-OH-TRZ, and DEX were obtained from commercial sources or were provided by their pharmaceutical manufacturers. Cofactors $NADP^+$, DL-isocitric acid, $MgCl_2$, isocitric dehydrogenase, and potassium phosphate buffer solutions were purchased from Sigma. In quantitative western blot assays, the primary antibody was rabbit anti-rat CYP3A1 (Xenotech), and the secondary antibody was polyclonal donkey anti-rabbit Ig linked to horseradish peroxidase (Amersham).

Microsomal Preparation

Mouse livers were taken from three *mdr1a* (−/−) mice, one *mdr1a/b*(−/−) mouse, and four matched *mdr1a/b*(+/+) controls (Taconic Farms). All liver microsomes were prepared by ultracentrifugation as previously described [17]. Total protein concentration was determined by a bicinchoninic acid protein assay (BCA; Pierce Chemical Co.), with BSA as a standard.

Incubation Procedures

Incubation mixtures contained 50 mmol/L of phosphate buffer, 5 mmol/L of Mg^{2+}, 0.5 mmol/L of $NADP^+$, and an isocitrate/isocitric dehydrogenase regenerating system. MDZ in methanol solution was aliquoted into incubation tubes to yield final incubate concentrations ranging from 0 to 250 μM. Due to limited quantities of microsomes, TRZ and DEX in methanol solution was aliquoted to yield a single final incubate concentration of 500 μM TRZ and 20 μM DEX. The solvent was evaporated to dryness at 40° under conditions of mild vacuum. Incubations were initiated by the addition of microsomal protein (0.5 mg/mL), and samples were incubated with agitation for 5 (MDZ), 20 (TRZ), and 30 (DEX) min at 37°. Reactions were stopped by cooling on ice and the addition of acetonitrile. All samples were assayed in duplicate. Phenacetin (250 ng) was added as an internal standard to MDZ and TRZ samples and tacrine (25 ng) to DEX samples, the incubation mixture was centrifuged, and the supernatant was transferred to an autosampling vial for HPLC analysis. Formation of metabolites for MDZ, TRZ, and DEX was linear with respect to incubation time and microsomal protein concentration. Throughout all experiments, control incubations with 5 μM ketoconazole and without cofactor, protein, and/or drug substrate were performed to validate CYP3A-mediated metabolism.

Metabolite Detection, HPLC

For detection of MDZ/TRZ and their metabolites, the HPLC mobile phase consisted of 200 mL of acetonitrile, 350 mL of methanol, and 450 mL of 10 mmol/L of phosphate buffer; the flow rate was 1.4 mL/min. The analytical column was stainless steel, 30 cm × 3.9 mm, containing reverse-phase C-18 μBondapak (Waters Associates). Column effluent was monitored by ultraviolet absorbance at 220 nm. For detection of DEX and its metabolites, the HPLC mobile phase consisted of 250 mL of acetonitrile, 750 mL of 10 mmol/L of phosphate buffer; pH was adjusted to 3 with HCl; the flow rate was 1.4 mL/min. The analytical column was stainless steel, 30 cm × 3.9 mm, containing reverse-phase C-18 μBondapak (Waters Associates). Column effluent was monitored by ultraviolet absorbance at 240 nm. The identities of the MDZ/TRZ metabolites were verified by comparing retention time with authentic standards.

Data Analysis

Formation rates of α-OH-MDZ and 4-OH-MDZ in reaction mixtures were determined based on calibration curves constructed from a series of standards containing various amounts of α-OH-MDZ and 4-OH-MDZ together with internal standard using PHR quantification. Reaction velocities were calculated in units of nanomoles of product formed per minute per milligram of microsomal protein. Formation rate and reaction velocities of α-OH-TRZ and 4-OH-TRZ were calculated similarly, using α-OH-TRZ and 4-OH-TRZ standards. The kinetics of MDZ 4-hydroxylation were determined using nonlinear regression based on a

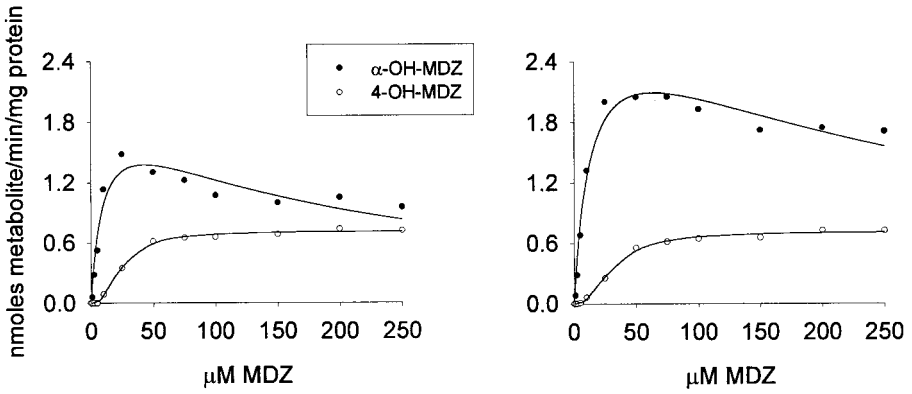

FIG. 1. Rates of formation of α-OH- and 4-OH-MDZ in relation to concentrations of the substrate MDZ by microsomal preparations of a representative *mdr1a/b(+/+)* (left) and an *mdr1a(−/−)*mouse (right) sample. Lines represent functions determined by nonlinear least squares regression analysis.

substrate activation (Hill) model, as evident from graphic analysis of reaction velocity versus substrate concentration and reciprocal (Eadie–Hofstee) plots [18, 19]. For α-OH-MDZ, plots of V versus S and reciprocal plots demonstrated diminished reaction velocities at high substrate concentrations. This pattern was described previously for α-OH-MDZ [18, 20] and is consistent with Michaelis–Menten kinetics and uncompetitive substrate inhibition [21]. Accordingly, the kinetics of MDZ α-hydroxylation were determined using nonlinear regression based on a Michaelis–Menten model with uncompetitive substrate inhibition [18, 21]. Because reference standards of DEX metabolites were not available, DEX metabolite formation rates were expressed in relative units of PHR, specifically the metabolite peak height divided by the peak height of the internal standard, tacrine.

Quantitative Western Blot

Microsomal protein was separated by SDS–PAGE as described by Laemmli [22] in 7.5% polyacrylamide gels. In brief, sample wells were loaded with 1.0 μg of microsomal protein. Human cDNA expressed CYP3A4 (Gentest) was used to generate calibration standards at concentrations of 0.5, 1.2, and 3.75 pmol/well. Samples were run at 80 V for 2 hr in 25 mM Tris buffer/0.1% SDS buffer. Then samples were transferred to Immobilon-P (PVDF membrane) (Millipore) for 1 hr at 100 V in 25 mM Tris buffer/20% methanol. Blots were blocked with 3% dry milk for 1 hr, incubated with a polyclonal rabbit anti-rat CYP3A1 (1:3000) (Xenotech) for 1 hr, and then reblocked for 30 min. Next the blots were probed with the secondary antibody, donkey anti-rabbit Ig-horseradish peroxidase (1:6000) (Amersham) for 1 hr. The Super Signal Cl-HRP Substrate System (Pierce) was used to activate the HRP signal, and then blots were exposed to film (see Fig 2A). Quantitation of protein was completed via computer image analysis (Image Pro Plus, Media Cybernetics). A standard curve of pixel area · density versus picomoles of CYP3A4 was created and fit to the equation $y = mx^A$ using nonlinear least squares regression (see Fig. 2B).

RESULTS

Both α-OH- and 4-OH-MDZ were formed by *mdr1a(−/−)*, *mdr1a/b(−/−)* and *mdr1a/b(+/+)* mouse liver microsomes (Fig. 1). Ketoconazole (5 μM) inhibited α-hydroxylation of MDZ less than 50%, indicating that the α-hydroxylation is not completely dependent on CYP3A isoform activity in mice (unpublished data); furthermore, α-OH-MDZ formation has demonstrated lower susceptibility to classic CYP3A inhibitors, troleandomycin and ketoconazole, in rats [23]. In any case, the α-OH-MDZ kinetic parameters for *mdr1a(−/−)* and *mdr1a/b(+/+)* mice were similar (Table 1), but V_{max} was actually increased in *mdr1a(−/−)* mice. The 4-hydroxylation of MDZ was virtually elimi-

TABLE 1. Summary of biotransformation of MDZ in *mdr1a/b (+/+)*, *mdr1a(−/−)*, and *mdr1a/b(−/−)* mice

	α-OH-MDZ Formation	4-OH-MDZ Formation
mdr1a/b(+/+) (N = 4)		
V_{max}*	2.26 ± 0.17	0.69 ± 0.08
K_m†	9.3 ± 1.9	25.4 ± 0.6
K_s†	191.0 ± 14.6	
A		1.98 ± 0.16
V_{max}/K_m ratio‡	0.28 ± 0.042	0.030 ± 0.003
mdr1a(−/−) (N = 3)		
V_{max}*	3.22 ± 0.36	0.78 ± 0.12
K_m†	13.4 ± 2.6	35.5 ± 4.1
K_s†	280 ± 23.1	
A		1.93 ± 0.21
V_{max}/K_m ratio‡	0.26 ± 0.027	0.024 ± 0.003
mdr1a/b(−/−) (N = 1)		
V_{max}*	2.24	0.75
K_m†	8.3	18.9
K_s†	2.55	
A		1.86
V_{max}/K_m ratio‡	0.27	0.040

Values are means ± SEM. V_{max}, maximum reaction velocity; K_m, substrate concentration corresponding to 50% of V_{max}; K_s, substrate inhibition constant; A, Hill equation exponent.

* Expressed in nmol/min/mg protein.

† Expressed in μM.

‡ Expressed in mL/min/mg protein.

TABLE 2. Velocity of TRZ metabolite formation in *mdr1a/b(+/+)*, *mdr1a(−/−)*, and *mdr1a/b(−/−)* mice at TRZ = 500 μM

	α-OH-TRZ Formation	4-OH-TRZ Formation
mdr1a/b(+/+) (N = 4)	1.83 ± 0.02	2.01 ± 0.03
mdr1a(−/−) (N = 3)	2.23 ± 0.03	2.29 ± 0.03
mdr1a/b(−/−) (N = 1)	1.91	1.73

Values are means ± SEM. Units are nmol/min/mg protein.

nated with 5 μM ketoconazole, suggesting high dependence of the CYP3A isoform for 4-OH-MDZ production. The 4-OH-MDZ kinetic parameters for *mdr1a(−/−)* and *mdr1a/b(+/+)* mice were not significantly different (Fig. 1, Table 1). α-OH- and 4-OH-MDZ kinetics were evaluated for one *mdr1a/b(−/−)* mouse, along with an *mdr1a/b(+/+)* control, and were found to have kinetics similar to those of the *mdr1a/b(+/+)* liver microsomes (Table 1).

TRZ biotransformation yields two major metabolites, α-OH-TRZ and 4-OH-TRZ. TRZ metabolite formation was inhibited by ketoconazole with a profile similar to that of MDZ metabolite formation. TRZ biotransformation was investigated at 500 μM, a concentration that exceeds the K_m for both pathways [19, 24]. There was no difference in reaction velocity between *mdr1a(−/−)* or *mdr1a/b(−/−)* and *mdr1a/b(+/+)* controls (Table 2).

DEX metabolites were formed by *mdr1a(−/−)*, *mdr1a/b(−/−)*, and *mdr1a/b(+/+)* mouse liver microsomes, producing five major metabolites. Ketoconazole (5 μM) inhibited all DEX metabolite formation to some degree; however, metabolites M1 and M5 were inhibited the most (94 and 70%, respectively), and their formation was considered to be dependent on the CYP3A isoforms. The production of five major DEX metabolites with sensitivity to ketoconazole inhibition agrees with previously published data [25]. The M1 and M5 PHR values for *mdr1a(−/−)* and *mdr1a/b(+/+)* mice were not significantly different, while the PHR values for M2, M3, and M4 in *mdr1a(−/−)* appeared higher than in the *mdr1a/b(+/+)*controls (Table 3).

Western blotting detected two proteins, most likely CYP3A11 and CYP3A13 (Fig. 2A). Both bands were quantified by computer image analysis, and no significant difference was seen in the amount of CYP3A immunoreactive protein in *mdr1*-deficient mice (band 1: 1.31 ± 0.19; band 2: 1.38 ± 0.15 pmol/μg protein) compared to controls (band 1: 1.30 ± 0.18; band 2: 1.36 ± 0.11 pmol/μg protein) (Fig. 2C).

DISCUSSION

P-gp is not directly involved in substrate biotransformation. However, the export of xenobiotic by P-gp in the intestine, kidney, and liver may influence drug absorption and clearance [15, 26]. Presumably, by pumping substrates from the cells into the lumina of clearance organs, P-gp causes more parent drug or locally metabolized drug (at the level of the intestine or kidney) to be excreted [6, 26, 27]. P-gp has considerable substrate overlap with CYP3A [5], as well as similarities in chemical inhibition and induction [5, 8, 10]. This, along with the proximal location of CYP3A and P-gp on the same chromosome, has raised the possibility of co-regulation of P-gp and CYP3A [5, 8, 10, 12, 13, 15, 26, 28]. However, *in vitro* kinetic data indicated that conversion of MDZ to 4-OH-MDZ was not different between control and P-gp-deficient animals. The V_{max} of α-OH-MDZ was increased in P-gp-deficient mice; however, α-OH-MDZ formation studies with classic CYP3A inhibitors suggest that α-OH-MDZ production is not mediated entirely by CYP3A in rats and mice [23]. In general, the production of the major metabolites of MDZ (α-OH- and 4-OH-MDZ) was similar to that found in previous *in vitro* studies in humans and rats [18, 20, 23]. TRZ biotransformation, at a concentration exceeding the K_m, further validated that CYP3A metabolism is unaltered in P-gp-deficient mice. Formation of the DEX metabolites M1 and M5 showed no difference between control and P-gp-deficient mice. Considering that MDZ and TRZ are non-P-gp substrates, while DEX is, it appears that CYP3A-mediated metabolism was unaffected by the *mdr(−/−)* genotype, regardless of the P-gp substrate profile. Interestingly, metabolite formation that could not be verified as completely dependent on CYP3A (α-OH-MDZ/TRZ, M2, M3, M4) all appeared elevated in *mdr1a(−/−)* mice (Tables 1–3). This may suggest that the P-gp deficiency is associated with increased activity of another CYP isoform in the *mdr1a(−/−)* mouse liver.

Along with metabolic activity data, quantitation of immunoreactive CYP3A proteins in P-gp-deficient mice and controls revealed no difference. Polyclonal anti-rat CYP3A1 antibody was used to detect mouse CYP3A isoforms, and two bands were visualized. The most probable proteins detected were CYP3A11 and CYP3A13, which are the major CYP3A isoforms in mice [29]. The rat CYP3A1 used to generate the detection antibody has 87 and 70% amino acid sequence homology with mouse CYP3A11 and CYP3A13, respectively [29, 30]. Due to the similarity in

TABLE 3. DEX metabolite formation in *mdr1a/b(+/+)*, *mdr1a(−/−)*, and *mdr1a/b(−/−)* mice at DEX = 20 μM

	M1	M2	M3	M4	M5
mdr1a/b(+/+) (N = 4)	0.473 ± 0.049	0.164 ± 0.029	0.041 ± 0.008	0.120 ± 0.027	0.055 ± 0.002
mdr1a(−/−) (N = 3)	0.477 ± 0.043	0.260 ± 0.018	0.077 ± 0.007	0.206 ± 0.009	0.046 ± 0.006
mar1a/b(−/−) (N = 1)	0.695	0.1997	0.033	0.136	0.044

Values are presented as the mean peak-height ratio ± SEM.

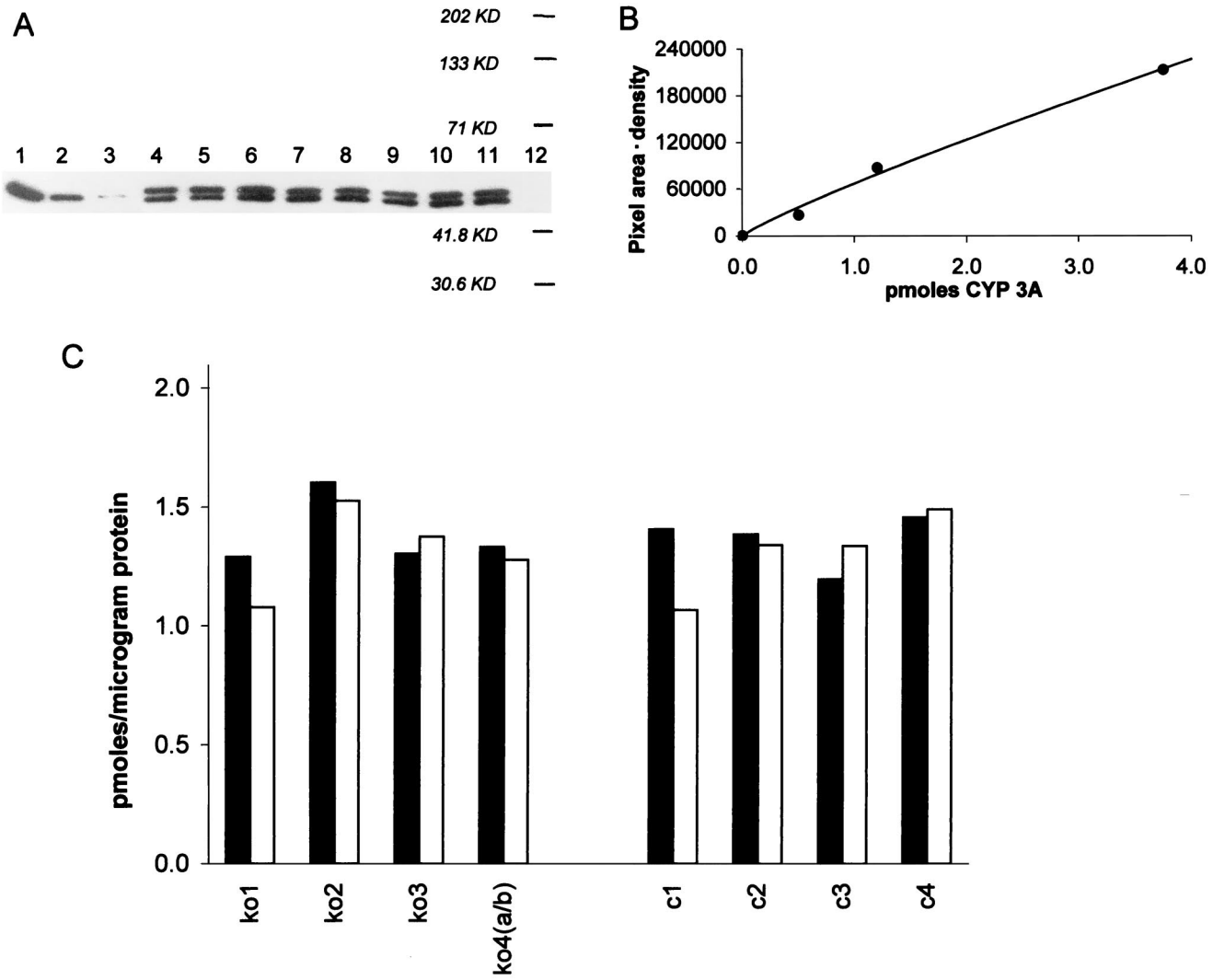

FIG. 2. Immunoquantification of CYP3A in P-gp-deficient [*mdr1a(−/−), mdr1a/b(−/−)*] and control [*mdr1a/b (+/+)*] mice. Rabbit anti-rat CYP3Al antibody (Xenotech) was used as a primary antibody in immunoblot detection (A). Lanes 1 through 3: 3.75, 1.2, and 0.5 pmol cDNA expressed CYP3A4, respectively. Lanes 4, 6, and 8: 1.0 μg of *mdr1a(−/−)* microsomal preparation. Lanes 5, 7, 9, and 11: 1.0 μg of control [*mdr1a/b(+/+)*] microsomal liver preparation. Lane 10: 1.0 μg of *mdr1a/b(−/−)* microsomal preparation. Each lane represents a sample from an individual mouse. Lane 12: Molecular weight markers. Known amounts of cDNA expressed human CYP3A4 (Gentest) were used to generate a standard curve (B). Each animal sample was analyzed via computer image scanning and then quantified by comparison to the standard curve (pixel area · pixel density). The bar graph (C) represents quantities of immunoreactive hepatic CYP3A in individual samples of P-gp-deficient mice [*mdr1a(−/−)* or *mdr1a/b(−/−)*, ko1 through ko4] and in matched controls [*mdr1a/b(+/+)*, c1 though c4]. Solid bars represent the upper band (band 1); open bars represent the lower band (band 2). Mean quantities for the two groups are nearly identical.

molecular weight (CYP3A11: M_r = 57,853; CYP3A13: M_r = 57,491) [29, 30], the protein bands migrated close together (Fig. 2A). However, on the original film exposure, two distinct bands were discernible. Similar results for immunodetection of mouse CYP3A have been described [13].

P-gp has substrate specificity similar to that of CYP3A, and is modulated by some of the same chemical inducers and inhibitors of CYP3A [5, 8, 10]. *In vivo* studies indicate that disruption of the *mdr1* gene, or chemical inhibition of P-gp, may influence xenobiotic clearance indirectly [15, 26]. However, genetic disruption of the *mdr1* genes to create P-gp-deficient mice does not affect CYP3A-mediated kinetics or protein expression.

This work was supported by Grants MH-34223, MH-01237, MH-19924, and DA-05258 from the Department of Health and Human Services.

References

1. Borst P, Schinkel AH, Smit JJ, Wagenaar E, Van Deemter L, Smith AJ, Eijdems EW, Baas F and Zaman GJ, Classical and novel forms of multidrug resistance and the physiological functions of P-glycoproteins in mammals. *Pharmacol Ther* **60:** 289–299, 1993.
2. Silverman JA and Schrenk D, Hepatic canalicular membrane 4: Expression of the multidrug resistance genes in the liver. *FASEB J* **11:** 308–313, 1997.
3. Schinkel AH, Wagenaar E, Mol CA and van Deemter L,

P-glycoprotein in the blood-brain barrier of mice influences the brain penetration and pharmacological activity of many drugs. *J Clin Invest* **97:** 2517–2524, 1996.
4. Gottesman MM, Pastan I and Ambudkar SV, P-glycoprotein and multidrug resistance. *Curr Opin Genet Dev* **6:** 610–617, 1996.
5. Wacher VJ, Wu CY and Benet LZ, Overlapping substrate specificities and tissue distribution of cytochrome P450 3A and P-glycoprotein: Implications for drug delivery and activity in cancer chemotherapy. *Mol Carcinog* **13:** 129–134, 1995.
6. Watkins PB, The barrier function of CYP3A4 and P-glycoprotein in the small bowel. *Adv Drug Delivery Rev* **27:** 161–170, 1997.
7. Schinkel AH, Smit JJM, van Tellingen O, Beijnen JH, Wagenaar E, van Deemter L, Mol CAAM, van der Valk MA, Robanus-Maandag EC, te Riele HPJ, Berns AJM and Borst P, Disruption of the mouse *mdr1a* P-glycoprotein gene leads to a deficiency in the blood–brain barrier and to increased sensitivity to drugs. *Cell* **77:** 491–502, 1994.
8. Wacher VJ, Salphati L and Benet LZ, Active secretion and enterocytic drug metabolism barriers to drug absorption. *Adv Drug Delivery Rev* **20:** 99–112, 1996.
9. Tsui LC, Donis-Keller H and Grzeschik KH, Report of the second international workshop on human chromosome 7 mapping 1994. *Cytogenet Cell Genet* **71:** 2–21, 1995.
10. Schuetz EG, Beck WT and Schuetz JD, Modulators and substrates of P-glycoprotein and cytochrome P4503A coordinately up-regulate these proteins in human colon carcinoma cells. *Mol Pharmacol* **49:** 311–318, 1996.
11. Lee CH, Bradley G, Zhang JT and Ling V, Differential expression of P-glycoprotein genes in primary rat hepatocyte culture. *J Cell Physiol* **157:** 392–402, 1993.
12. Salphati L and Benet LZ, Modulation of P-glycoprotein expression by cytochrome P450 3A inducers in male and female rat livers. *Biochem Pharmacol* **55:** 387–395, 1998.
13. Schuetz EG, Schinkel AH, Relling MV and Schuetz JD, P-glycoprotein: A major determinant of rifampicin-inducible expression of cytochrome P4503A in mice and humans. *Proc Natl Acad Sci USA* **93:** 4001–4005, 1996.
14. Ford JM and Hait WN, Pharmacologic circumvention of multidrug resistance. *Cytotechnology* **12:** 171–212, 1993.
15. Schinkel AH, Wagenaar E, van Deemter L, Mol CA and Borst P, Absence of the mdr1a P-glycoprotein in mice affects tissue distribution and pharmacokinetics of dexamethasone, digoxin, and cyclosporin A. *J Clin Invest* **96:** 1698–1705, 1995.
16. von Moltke LL, Granda BW, Grassi JM and Greenblatt DJ, Multiple site interaction of triazolam and ketoconazole in mice: Role of P-glycoprotein. *Clin Pharmacol Ther* **65**: 143, 1999.
17. von Moltke LL, Greenblatt DJ, Harmatz JS and Shader RI, Alprazolam metabolism *in vitro:* Studies of human, monkey, mouse, and rat liver microsomes. *Pharmacology* **47:** 268–276, 1993.
18. von Moltke LL, Greenblatt DJ, Schmider J, Duan SX, Wright CE, Harmatz JS and Shader RI, Midazolam hydroxylation by human liver microsomes *in vitro*: Inhibition by fluoxetine, norfluoxetine, and by azole antifungal agents. *J Clin Pharmacol* **36:** 783–791, 1996.
19. Fahey JM, Pritchard GA, Moltke LL, Pratt JS, Grassi JM, Shader RI and Greenblatt DJ, Effects of ketoconazole on triazolam pharmacokinetics, pharmacodynamics and benzodiazepine receptor binding in mice. *J Pharmacol Exp Ther* **285:** 271–276, 1998.
20. Kronbach T, Mathys D, Umeno M, Gonzalez FJ and Meyer UA, Oxidation of midazolam and triazolam by human liver cytochrome P450IIIA4. *Mol Pharmacol* **36:** 89–96, 1989.
21. Segel IH, *Enzyme Kinetics*. Wiley, New York, 1975.
22. Laemmli VK, Cleavage of structural proteins during the assembly of the head of bacteriophage T4. *Nature* **227:** 680–685, 1970.
23. Ghosal A, Satoh H, Thomas PE, Bush E and Moore D, Inhibition and kinetics of cytochrome P4503A activity in microsomes from rat, human, and cDNA expressed human cytochrome P450. *Drug Metab Dispos* **24:** 940–947, 1996.
24. von Moltke LL, Greenblatt DJ, Harmatz JS, Duan SX, Harrel LM, Cotreau-Bibbo MM, Pritchard GA, Wright CE and Shader RI, Triazolam biotransformation by human liver microsomes *in vitro*: Effects of metabolic inhibitors and clinical confirmation of a predicted interaction with ketoconazole. *J Pharmacol Exp Ther* **276:** 370–379, 1996.
25. Tomlinson ES, Maggs JL, Park BK and Back DJ, Dexamethasone metabolism *in vitro:* Species differences. *J Steroid Biochem Mol Biol* **62:** 345–352, 1997.
26. Lown KS, Mayo RR, Leichtman AB, Hsiao HL, Turgeon DK, Schmiedlin-Ren P, Brown MB, Guo W, Rossi SJ, Benet LZ and Watkins PB, Role of intestinal P-glycoprotein (mdr1) in interpatient variation in the oral bioavailability of cyclosporine. *Clin Pharmacol Ther* **62:** 248–260, 1997.
27. Haehner BD, Gorski JC, Vandenbranden M, Wrighton SA, Janardan SK, Watkins PB and Hall SD, Bimodal distribution of renal cytochrome P450 3A activity in humans. *Mol Pharmacol* **50:** 52–59, 1996.
28. Pfeil D, Bergmann J, Fichtner I, Stein U, Hentschel M, Rothe I and Goan SR, Multidrug resistance of murine leukemia cells characterization and correlation with cytochrome P-450 dependent activities, cytosolic calcium and cell cycle state. *Anticancer Res* **14:** 571–576, 1994.
29. Yanagimoto T, Itoh S, Sawada M, Hashimoto H and Kamataki T, Molecular cloning and functional expression of a mouse cytochrome P-450 (Cyp3a-13): Examination of Cyp3a-13 enzyme to activate aflatoxin B_1 (AFB_1). *Biochim Biophys Acta* **1201:** 405–410, 1994.
30. Yanagimoto T, Itoh S, Muller-Enoch D and Kamataki T, Mouse liver cytochrome P-450 (P-450IIIAm1): Its cDNA cloning and inducibility by dexamethasone. *Biochim Biophys Acta* **1130:** 329–332, 1992.